

Improving 2D mesh image segmentation with Markovian Random Fields

Alex J. Cuadros-Vargas, Leandro C. Gerhardinger, Mário de Castro
João Batista Neto and Luis Gustavo Nonato
Instituto de Ciências Matemáticas e de Computação - USP
CP 668, São Carlos, SP, Brazil 13560-970
alexj,leandro,mcastro,jbatista,gnonato@{icmc.usp.br}

Abstract

Traditional mesh segmentation methods normally operate on geometrical models with no image information. On the other hand, 2D image-based mesh generation and segmentation counterparts, such as Imesh [6] perform the task by following a set of well defined rules derived from the geometry of the triangles, but with no statistical information of the mesh elements.

This paper presents a novel segmentation method that combines the original Imesh image-based segmentation approach with Markovian Random Field (MRF) models. It takes an image as input, generate a mesh of triangles and, by treating the mesh as a Markovian field, produces quality unsupervised segmentation.

The results have demonstrated that the method not only provides better segmentation than that of original Imesh, but is also capable of producing MRF-like segmentation output for certain types of images, with considerable cut in processing times.

1 Introduction

Image segmentation by Markovian Random Field (MRF) models is an expanding research field. Traditionally, the attractiveness of the MRF approach to segmentation is its ability to correctly model images with texture patterns that exhibit random behaviour, providing good segmentation [13, 9]. Moreover, the process is accomplished in an unsupervised fashion and is also capable of representing many stochastic problem by modelling complex features with a relatively reduced number of parameters.

Applications of MRF to segmentation may range from remote sensing [23] to medicine [22] and are commonly applied to 2D data. However, some results can be found in the 3D domain. Chistopher [4] has developed a MRF segmentation method for inherent 3D medical data, such as Computed Tomography and Magnetic Resonance Imaging.

In the MRF approach to segmentation, an image is represented by the capture of local features, determining for every pixel in the image its grey level dependence with relation to its neighbours' grey level. This dependence is expressed in terms of a conditional probability distribution, computed over the intensity of each pixel. Any decomposition that possess neighbourhood relationships of such fashion and well established segmentation properties can be segmented by MRF.

A typical example of such decomposition are images represented by meshes, as neighbourhood relationships can easily be defined for them. Furthermore, meshes can be built so as to incorporate some specific features of the image, turning segmentation an easier and faster task. Another aspect is that images represented by meshes possess a reduced number of cells (when compared with that of pixel or voxel representations), demanding a lower computational effort in the segmentation process.

Traditionally, mesh segmentation methods operate on geometrical models with no image information attached [25, 14, 24]. Such methods aim to find structures of interest in the mesh suitable for computer vision applications.

In spite of good properties of mesh representation, the use of MRF in such decomposition has never been explored. Another important fact not usually considered is that mesh representation provides, as well as the traditional information required by MRF, additional geometrical information that can empower the MRF segmentation output. In fact, instead of solely looking at the pixel grey level, improved segmentation could be attained if MRF were combined with features provided by meshes such as area, edge length, cell aspect ratio and so on.

This paper presents a novel unsupervised 2D segmentation method that combines both MRF and meshes. The method extends the concept of MRF segmentation, traditionally focused on pixel local features and its neighbourhood, to a broader framework in which features extracted from meshes are also considered in the computation of the segmented image. The results have shown a significant im-

provement in the quality of the final segmentation when compared with that accomplished with a set of well defined mesh segmentation rules alone, the original Imesh. Also, the new method exhibits much lower segmentation times in comparison with traditional MRF segmentation methods.

This paper is organised as follows. Section 2 describes the MRF image segmentation method. The concepts and the decomposition process for the mesh generation are described in section 3. The combination of both MRF and mesh is introduced in section 4 and some results are presented in section 5. Conclusions are finally found in section 6.

2 Markovian Random Field Model to segmentation

Many objects in real images are characterised by texture of random or non deterministic behaviour. For such cases a probabilistic approach to segmentation can be desirable. Many works on stochastic models for images have been developed [12, 7, 13, 5] and successfully applied in different situations [18, 1, 2, 21].

For such models, objects in a digital image are seen as a group of pixels enclosed in a given area. The representation of each object can be done by labelling them and constructing a label field. Generally, stochastic segmentation algorithms define such labels as random variables, grouped into a so called 2D random field.

Many random field models exist [19] such as Gibbs, Ising, Potts, Pickard and Markov. The latter, is very adequate for modeling texture (especially micro-texture) for that it defines a probability function for the field by means of purely local features, ie, neighbouring features.

Unsupervised segmentation by stochastic models belongs to the family of incomplete data problems. Hence, the segmentation task is, in the end, a problem of statistical optimization of a given criterion. In this model the image to be segmented is the *observed data*; the results sought, normally named class map or label field, is considered the *missing data* and; the set of *model parameters* is an item to be computed. The implementation of such approach comprises a two-fold process: a) parameter estimation and b) the statistical optimization itself.

The parameter estimation process can be accomplished by some iterative algorithms: EM (Expectation Maximization), SEM (Stochastic Estimation-Maximization) and ICE (Iterative Conditional Estimation). For the statistical optimization, two processes are known: MAP (Maximization a Posterior) [7, 15] and MPM (Maximizer of the Posterior Marginals) [16, 5], which is more appropriate to image segmentation than MAP [16]. While the latter assigns the same cost for every incorrect segmentation over the entire image, the former assigns a cost based on the number of misclassi-

fied pixels. This work has adopted the EM/MPM approach as proposed by Comer [5]. The approach will be briefly described in the next section.

2.1 The EM/MPM segmentation

In the Markovian EM/MPM image segmentation method, the observed data is the observed image, given by $\mathbf{Y} = Y_1, \dots, Y_N$ and the label field $\mathbf{X} = X_1, \dots, X_N$ is the missing data. \mathbf{X} and \mathbf{Y} are 2D random fields of a rectangular grid S with N variables. According to Bayes' Theorem, the posterior probability $p_{\mathbf{X}|\mathbf{Y}}$ is proportional to the prior probability $p_{\mathbf{X}}$ times a likelihood function $f_{\mathbf{Y}|\mathbf{X}}$. Hence,

$$p_{\mathbf{X}|\mathbf{Y}}(\mathbf{x}|\mathbf{y}, \boldsymbol{\theta}) \propto p_{\mathbf{X}}(\mathbf{x}) \times f_{\mathbf{Y}|\mathbf{X}}(\mathbf{y}|\mathbf{x}, \boldsymbol{\theta}), \quad (1)$$

where $\boldsymbol{\theta}$ is the parameter array for the model and $\mathbf{y} = y_1, \dots, y_n$ and $\mathbf{x} = x_1, \dots, x_n$ are sample realizations of \mathbf{Y} and \mathbf{X} , respectively. Each x_s can be assigned the value of a label $k = 1, \dots, L$, with L being the number of labels previously defined. On the other hand, y_s are grey levels in the range $0, \dots, 255$.

The segmentation methods seeks to find an estimate for the label field \mathbf{x} through the MPM optimization method, whose minimization criterion is the expected number of mislabelled pixels. As an unsupervised segmentation method, the EM algorithm is then employed to estimate the parameters $\boldsymbol{\theta}$ of the model.

In the original formulation proposed by Comer and Delp [5] for image segmentation, the probability $f_{Y_s|X_s}, \forall s \in \{1, \dots, N\}$ is considered a normal distribution that only depends on X_s . Hence,

$$\begin{aligned} f_{\mathbf{Y}|\mathbf{X}}(\mathbf{y}|\mathbf{x}, \boldsymbol{\theta}) &= \prod_{s=1}^N f_{Y_s|X_s, \boldsymbol{\theta}}(y_s|x_s, \boldsymbol{\theta}) \\ &= \prod_{s=1}^N \frac{1}{\sqrt{2\pi\sigma_{x_s}^2}} \exp\left(-\frac{(y_s - \mu_{x_s})^2}{2\sigma_{x_s}^2}\right). \end{aligned} \quad (2)$$

The array of parameters $\boldsymbol{\theta}$ are the means and variance of each label, ie, $\boldsymbol{\theta} = [\mu_1, \sigma_1^2, \dots, \mu_L, \sigma_L^2]$. The distribution $p_{\mathbf{X}}$ of the label field is a Markovian Random Field [19, 8] that, according to Hammersley-Clifford's theorem [3, 12], has a conditional probability mass function given as a Gibbs distribution

$$p_{\mathbf{X}}(\mathbf{x}) = \frac{1}{Z} \exp(-U(\mathbf{x})), \quad (3)$$

where Z is a normalisation factor and $U(\mathbf{x})$ is an energy function in the form

$$U(\mathbf{x}) = \sum_{c \in C} V_c(\mathbf{x}). \quad (4)$$

$V_c(\mathbf{x})$ is a function that depends on the cliques and the family $\{V_c : c \in C\}$ is called potential. The set of pixels $C \subseteq S$ is a clique in the label field if, for any pixels $r, s \in C$, then $s \in \mathcal{G}_r$. That is, they are all neighbours. A collection $\mathcal{G} = \{\mathcal{G}_s \subseteq S, s \in S\}$ is a neighbouring system for S if, for any pixel in $s \in S$, then $s \notin \mathcal{G}_s$ and $s \in \mathcal{G}_r \iff r \in \mathcal{G}_s, \forall r \in S$. The elements of \mathcal{G}_s are then the neighbour pixels of a pixel s . Figure 1 shows a pixel and its 4- and 8-connected neighbourhood, with its respective cliques.

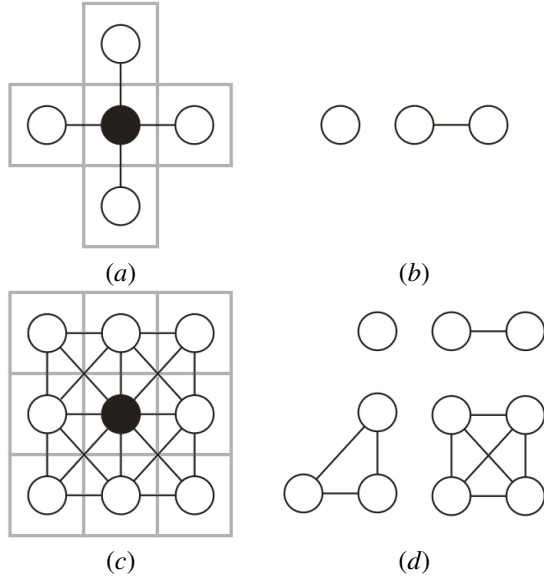


Figure 1. (a) 4-connected neighbourhood and (b) its corresponding cliques. (c) 8-connected neighbourhood and (d) its corresponding cliques.

For image segmentation purposes, an adequate energy function is given by

$$U(\mathbf{x}) = \sum_{\{r,s\} \in C} \beta t(x_r, x_s) + \sum_{\{r\} \in C} \gamma_r, \quad (5)$$

where

$$t(x_r, x_s) = \begin{cases} 0, & \text{if } x_r = x_s, \\ 1, & \text{if } x_r \neq x_s. \end{cases} \quad (6)$$

Notice that only the double cliques (two pixels) and single (one pixel) are taken into account in this model. The parameter β , called Spatial Interaction Parameter, defines a weight for the penalty function $t(x_r, x_s)$ of a double clique. This function aims to prevent neighbour pixel from having different labels. The set of parameters $\gamma_k, k = 1, \dots, L$, which acts upon the single cliques, can be considered as the occurrence costs of each label k . Since this is a unsupervised segmentation, the parameters γ_k are, generally, assumed to be 0, $\forall k$.

3 Mesh Generation

This section shows the process of mesh generation. Some basic definitions and terminologies are introduced, followed by the description of the mesh computation from an image.

3.1 Basic Concepts

Let S be a set of points in \mathbb{R}^2 . A *triangulation (mesh)* of S is a two-dimensional simplicial complex M whose vertices are the points of S , and any k -simplex of M , $k = 0, 1$, is contained in at least a 2-simplex (triangle) of M . If the union of all simplices in M makes up the convex hull of S and the circumcircle of each triangle in M does not contain in its interior any point of S then M is called *Delaunay triangulation* [10].

A *planar graph* is a graph G with vertices in \mathbb{R}^2 where each edge is a straight-line segment with ends in G and if e_1 and e_2 are two edges of G , $e_1 \cap e_2$ is either empty or a vertex of G . Given a planar graph G , a *mesh conformed by G* is a triangulation M where each vertex of G is in M and if e is an edge in G then $|e| = |e_1 \cup e_2 \cup \dots \cup e_k|$, where $e_i \in M$, $i = 1, \dots, k$ are edges of M and $|\cdot|$ represents the underlying space, i.e., each edge of G can appear subdivided as a set of edges in M .

Let S be a set of points and M be a mesh (triangulation) of S , if $M = M_1 \cup M_2 \cup \dots \cup M_k$, where each M_i is a triangulation and $M_i \cap M_j$, $i \neq j$ is either empty or a planar graph then $\{M_1, M_2, \dots, M_k\}$ is said a *k-partitioning* of M in *sub-meshes* M_i , $i = 1, \dots, k$.

An $m \times n$ *image* is a function $I : [0, \dots, m] \times [0, \dots, n] \rightarrow \mathbb{R}^+$ that assigns to each point $p \in [0, \dots, m] \times [0, \dots, n] \subset \mathbb{Z}^2$ a non-negative scalar $I(p)$. The pair $(p, I(p))$ is called pixel.

3.2 Image Mesh Decomposition

Image mesh decomposition concerns to the process of generating a mesh (triangulation) that fits features contained in the image. In our context, triangles should not be allowed to cross different regions of the image, that is, each triangle should be spatially contained in only one region of the image.

Let T be the set of triangles of a Delaunay triangular mesh M whose vertices are points of an image I and $E : T \rightarrow \mathbb{R}^+$ be a function that associates an error measure to each triangle in T . In fact, function E measures how good a triangle is regarding a specific property, that is, E enables to decide whether or not a triangle must belong to the triangulation.

Different strategies to define the function E have been presented in the literature, but usually such approaches rely on evaluating E by traversing all pixels inside a triangle

t so as to decide, based on some characteristic of the image, whether or not t is an appropriated triangle. In general, when E indicates that t is a bad triangle, the triangulation is updated by inserting new points within t , thus eliminating it from M [11].

Although widely employed, the bad triangles removal strategy described above presents two main drawbacks. Traversing all pixels within a triangle may demand a high computational cost. Each time the triangulation is updated all the new triangles must be scanned in order to evaluate E . Another concern is the insertion of new points in the triangulation. If not handled properly, this operation can result in an accumulation of points around already existing vertices.

To avoid the problems described above, we adopt an strategy based on the medians of the triangles to define the function E . By traversing medians only, one can reduce the computational effort while being effective in detecting triangles that go across different regions of the image.

Let h_1, h_2, h_3 be the three medians of a triangle $t \in M$. Consider the sets of points $P^{h_j} = \{p \in h_j \mid \mathcal{E}(p) \geq c_{\mathcal{E}}\}$ where \mathcal{E} is an edge detection operator and $c_{\mathcal{E}}$ is a user defined scalar. Therefore, P^{h_j} is the set of points where the edges of the image intersect the median h_j .

Let $\alpha_i, i = 1, 2, 3$ be the barycentric coordinates of a point $p_k \in P^{h_j}$ and $A(p_k) = \min\{\alpha_i\}$ be a function that associates to each p_k its smallest barycentric coordinate. Let $D_M(p_k)$ be the square distance between p_k and its closest vertex in M , that is, $D_M(p_k) = \min_{v_j \in M} \{d^2(p_k, v_j)\}$, where $d(\cdot, \cdot)$ is the Euclidean distance. p_{h_j} denotes the point of P^{h_j} where $D_M(p_k)$ is maximal. From these definitions, the error function E can be stated as follows:

$$E(t) = \max\{A(p_{h_j})\}, \quad j = 1, 2, 3 \quad (7)$$

Figure 2(b) gives a geometric interpretation of the function E . The barycentric coordinates of a point p_k is related with the areas of the triangles formed by p_k and the vertices of the triangle that contains p_k . Therefore, $A(p_{h_j})$ measures how much the area of a triangle t is enclosed within a region of the image. A small value of $A(p_{h_j})$ indicates that h_j intersects an edge of the image close to the boundary of the triangle. Thus, values of $E(t)$ close to zero indicate that t is well fitted within a region in the image. Hence, a triangle t is considered unsuitable if $E(t) > c_E$, where $0 \leq c_E \leq 1$ is a user defined scalar.

Unsuitable triangles are eliminated by inserting, in the Delaunay triangulation, the point p_{h_j} such that $E(t) = A(p_{h_j})$. Since p_{h_j} are points chosen to be as far as possible from the vertices of M , the problem of dense accumulation of points around existing vertices is reduced.

After the mesh generation process, segmentation can be performed by combining image attributes with topological and geometric information contained in the mesh so as to

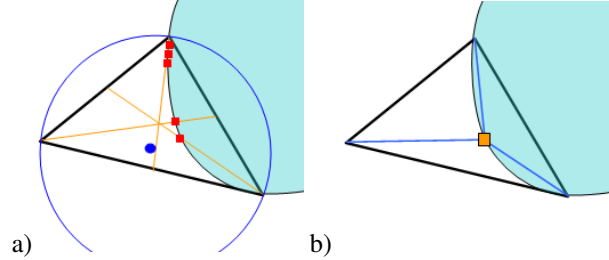


Figure 2. Error measure in a triangle. a) Detection of region borders, b) Geometric interpretation of the function E .

group cells into sub-meshes.

4 Mesh + MRF segmentation

This section shows how the traditional MRF segmentation model over neighbouring pixels can be extended to 2D mesh structures.

The greatest difference between mesh structures and images is in the geometry of the elements handled by both. Image pixels have the same shape, geometry and number of neighbours. 2D meshes, on the other hand, contain triangles of varied sizes, symmetry and a neighbourhood with different number of elements. Moreover, each neighbouring element may exhibit a wide-range adjacency degree. Figures 3(a) and 3(b) illustrate a general neighbouring scheme for a 2D mesh of a set of triangles and its respective cliques.

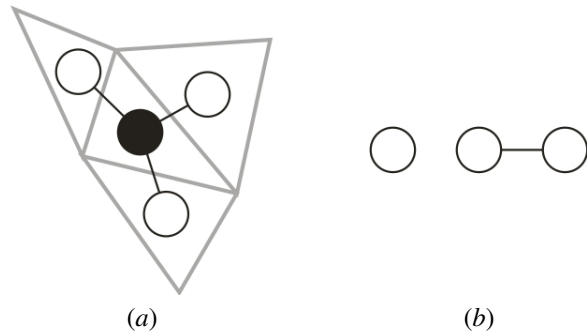


Figure 3. (a) Neighbourhood of a 2D mesh and (b) its corresponding cliques.

To handles mesh triangles, the original EM/MPM must be modified. The MPM estimation algorithm for the label field \mathbf{X} is extended so as to assign a weight, whose value depends on the planar geometry shared by the triangle and its neighbours, to every neighbouring element of every triangle in the mesh. Equation (6) is then rewritten as:

$$t(x_r, x_s) = \begin{cases} 0, & \text{if } x_r = x_s, \\ \frac{a_{s,r}}{p_s}, & \text{if } x_r \neq x_s, \end{cases} \quad (8)$$

where $a_{s,r}$ is the length of the edge shared by the triangles s and r , whereas p_s is the perimeter of s .

The parameter estimation algorithm EM is also altered. For an image, the intensity of each pixel has the same importance (weight) in the process. Mesh triangles, however, due to their varied geometry may possess different weights. The estimates for the set of parameters θ , as described by Comer and Delp [5], becomes:

$$\mu_k(p) = \frac{\sum_{s=1}^N y_s P(X_s = k | \mathbf{Y} = \mathbf{y}, \theta(p-1)) \times \mathbf{a}_s}{\sum_{s=1}^N P(X_s = k | \mathbf{Y} = \mathbf{y}, \theta(p-1)) \times \mathbf{a}_s} \quad (9)$$

and

$$\sigma_k^2(p) = \frac{\sum_{s=1}^N (y_s - \mu_k(p))^2 P(X_s = k | \mathbf{Y} = \mathbf{y}, \theta(p-1)) \times \mathbf{a}_s}{\sum_{s=1}^N P(X_s = k | \mathbf{Y} = \mathbf{y}, \theta(p-1))} \quad (10)$$

and \mathbf{a}_s is the area of the triangle s , used as a weight for the computation of variance and mean values of grey level of each label k . This proposal is equivalent to dividing, in equation 2, the variance $\sigma_{x_s}^2$ by the area of the triangle.

5 Results

To best illustrate the benefits of the proposed method we provide results from MRF segmentation alone (as described in section 2 and the Imesh method [6], a image based mesh generation and segmentation technique with no MRF-like neighbourhood relationship (as described in section 3).

We then confront both of them with the results obtained from the proposed method, for different values of β (Eq. 5). This parameter governs the influence of the geometry over the Mesh+MRF segmentation, as stated in Eq. 8. When $\beta = 0$, the geometry information from Eq. 8 is not considered. In this paper, we refer to this segmentation as **Mesh+MRF with no geometry information**. When $\beta > 0$, not only the neighbouring relationship of the MRF model, but also geometry information is added to the segmentation process. The higher the β parameter, the more geometry information the model conveys. This segmentation is referred to as **Mesh+MRF with geometry information**.

The behaviour of the Mesh+MRF segmentation method for increasing values of β is illustrated in Figure 4. Figures

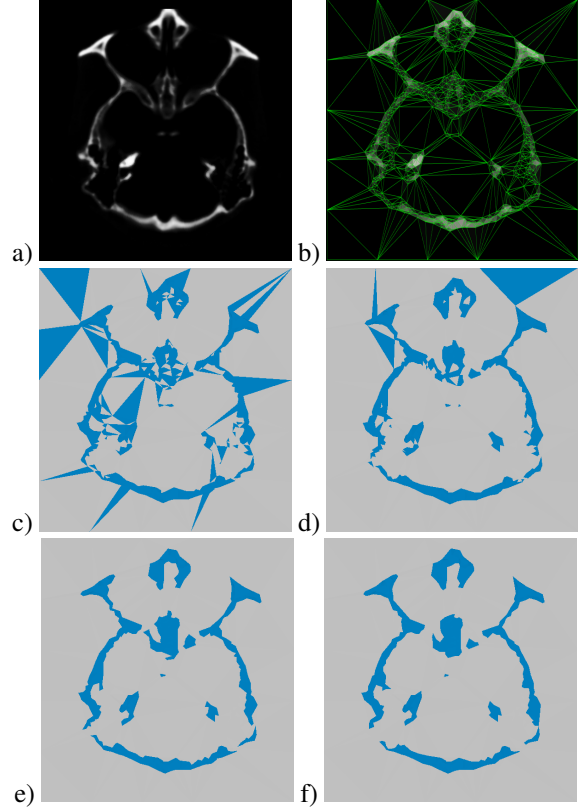


Figure 4. a) Original CT slice of a monkey head; b) Mesh Generated from (a); c) Mesh+MRF with no geometry information ($\beta = 0$). Mesh+MRF segmentation with geometry information: d) $\beta = 1$; e) $\beta = 2$; f) $\beta = 3$

4(a) and 4(b) are the original CT slice of a monkey head and its image-generated mesh, respectively. Figures 4(c), 4(d), 4(e) and 4(f) are the 2-class segmentation results for $\beta = 0, 1, 2$ and 3 , respectively. When $\beta = 0$, no geometry information from the triangles is considered and the segmentation is poor. As the value of β increases the perimeter and the length of the edge shared by neighbouring triangles become more relevant, yielding a smoother and more accurate segmentation.

Figure 5 illustrates the segmentation process (3 classes considered) for a CT scan slice of a foot. Figures 5(a) and 5(b) are, respectively, the original image and the mesh generated by the Imesh technique. Segmentation for the MRF method alone and Imesh (with no MRF model added) are given in 5(c) and 5(d), respectively. Images 5(e) and 5(f) are the results obtained with the Mesh+MRF segmentation without and with geometry information, respectively.

Notice how the segmentation from Mesh+MRF with geometry information is significantly more consistent than

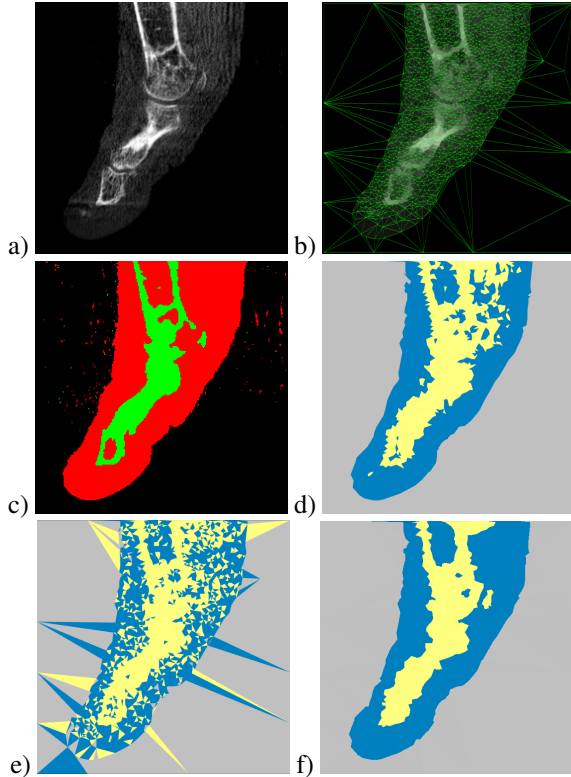


Figure 5. a) Original MRI image of a foot; b) Mesh Generated from (a); c) Segmentation by MRF alone; d) Mesh segmentation alone; e) Mesh+MRF segmentation with no geometry information; f) Mesh+MRF segmentation with geometry information ($\beta = 3$)

that computed from mesh segmentation without the MRF extension. Although not as good as the Markovian segmentation alone (Figure 5.c), due to the highly textural nature of the foot image, the result in 5(f) is an evidence of how an image-based mesh segmentation method can benefit from incorporating features originally designed for texture image segmentation such as MRF.

The final experiment of Figure 6 shows how the new method can contribute to shorten the processing time when compared with MRF segmentation alone. Image 6(a). is a high resolution (140x570) satellite image of the Superior lake on the Canadian border with the USA. Images 6(b) and 6(c) are, respectively, the segmentation results (2 classes) for the MRF alone and the Mesh+MRF method with geometry information, respectively. Although very similar in quality, the segmentation by the the new method is approximately 10x faster than that by MRF (see table 1).

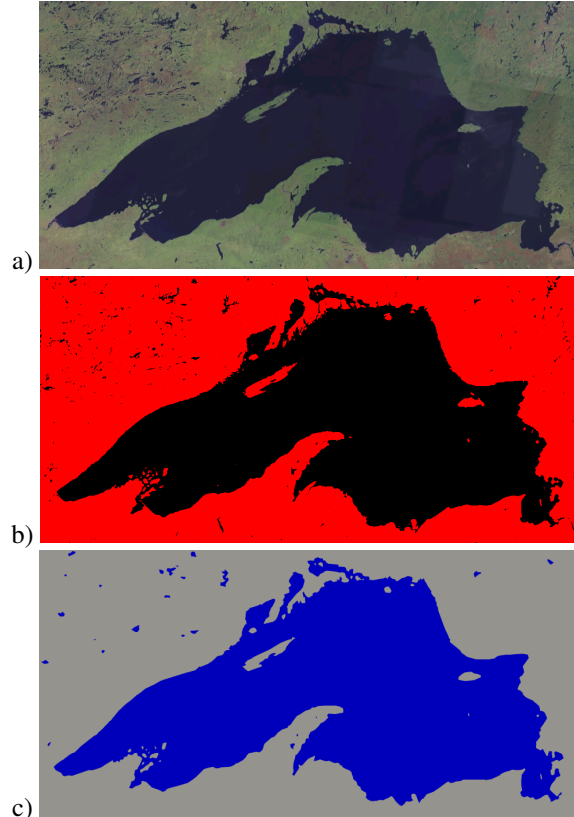


Figure 6. a) Original satellite image of a lake; b) Segmentation by MRF alone; c) Mesh+MRF segmentation with geometry information

6 Conclusions

This paper introduces a new method that combines MRF with Mesh to achieve image segmentation. Unlike traditional mesh segmentation techniques, which operate on geometrical models, our method takes an image as input, generate a mesh of triangles and, by treating this mesh as a Markovian field, produces quality unsupervised segmentation.

From the experiments we can devise two major contributions from this work. The first is the improvement in the quality of the segmentation when compared with the segmentation criteria so far available in the original Imesh method [6]. Such criteria did not take into account the statistical information now provided by the addition of the MRF functionality. The experiment of Figure 5 illustrates such behaviour. For image with some textural information and a considerable amount of noise, such that of the foot, the proposed method yields a more homogeneous segmentation than traditional Imesh, for example. However, as expected, for such kind of images the MRF segmentation

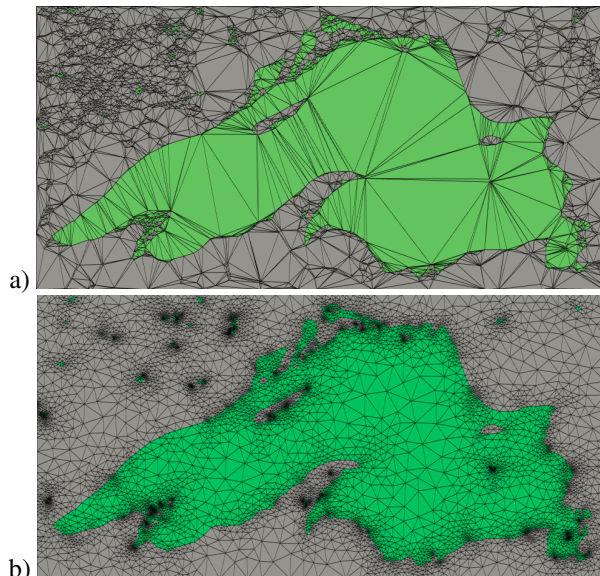


Figure 7. Meshes generated from fig. 6.a. a) Mesh employed in the segmentation of 6.c; b) Better quality mesh;

Image	MRF	Mesh+MRF		
		Mesh Gen.	Segment	Total
Monkey (256x256)	10	1.125	0.468	1.593
Foot (256x256)	12	1.263	1.375	2.638
Lake (1140x570)	90	6.64	2.343	8.983

Table 1. Segmentation times (in seconds) for the MRF and Mesh+MRF methods

method alone gives a better result. On the other hand, as demonstrates the experiment of Figure 6, the Mesh+MRF method can still provide comparable results with those of MRF alone for images with some textural information and irregular edges, provided the edges of the object sought are better delineated.

The second major contribution is a significant reduction in the segmentation times, especially when compared with MRF segmentation alone. As opposed to traditional MRF segmentation methods that operate on pixels, our approach deals with a mesh of triangles. Since the number of triangles of the mesh is much smaller than that of pixels in the corresponding image, the resulting segmentation is much faster. The values in table 1 give some evidences of this behaviour. Despite being a two-stage process (mesh generation and segmentation itself) the overall segmentation

times for the Mesh+MRF method are much smaller than those achieved with MRF method alone. The difference in processing times becomes more evident, for data of larger dimensions such as the satellite image of the lake. Reported segmentation time have been computed on a Xeon 3.2 GHz system, with 2GB RAM, running Windows.

Finally, it should be pointed out the ability of the method to incorporate quality criteria to the mesh elements [20, 17], while keeping the edges obtained during the segmentation process. Figure 7(a) shows the original mesh over the segmented image of the Lake 6(a). Figure 7(b) depicts a refined mesh derived from 7(a), with all edges preserved. A minimum angle value of 30° has been used as a quality criterion in this example.

Acknowledgements

We wish to acknowledge the Brazilian financial agencies CNPq (proc. 307268/2003-9, FAPESP (proc. 04/02810-0, 03/02815-0 and 02/05243-4) and CAPES involved in financing the project that generated these results.

References

- [1] A. Balan. Técnicas de segmentação de imagens aéreas para contagem de população de aves. Master's thesis, ICMC, Universidade de São Paulo, São Carlos, SP, Brasil, Fevereiro 2003.
- [2] A. Balan, A. Traina, C. Traina, and P. Azevedo. Fractal analysis of image textures for indexing and retrieval by content. pages 581–586. 18th IEEE Symposium on Computer-Based Medical Systems, June 2005.
- [3] J. Besag. Spatial interaction and the statistical analysis of lattice systems. *Journal of the Royal Statistical Society*, 36(2):192–236, 1974.
- [4] L. Christopher. *Bayesian segmentation of three dimensional images using the EM/MPM algorithm*. PhD thesis, Purdue University, 2003.
- [5] M. Comer and E. Delp. The em/mpm algorithm for segmentation of textured images: Analysis and further experimental results. *IEEE Transactions on Image Processing*, 9(10):1731–1744, October 2000.
- [6] A. Cuadros-Vargas, L. Nonato, M. R., and E. T. Imesh: An image based quality mesh generation technique. In *Brazilian Symposium on Computer Graphics and Image Processing, 18 (SIBGRAPI)*. IEEE Computer Society, 9–12 Oct. 2005.
- [7] H. Derin and H. Elliott. Modeling and segmentation of noisy and textured images using gibbs random fields. *IEEE Transactions on Pattern Analysis Machine Intelligence*, 9(1):39–55, 1987.
- [8] E. Dougherty. *Random Processes for Image and Signal Processing*. IEEE Series on Imaging Science and Engineering. SPIE/IEEE, 1998.
- [9] R. Fjortoft, W. Pieczynski, and Y. Delignon. Generalized mixture estimation and unsupervised classification based on hidden markov chains and hidden markov fields. *Scandinavian Conference on Image Analysis*, 2001.

- [10] S. Fortune. Voronoi diagrams and delaunay triangulation. In *Computing in Euclidean Geometry*, World Scientific Pub. Co., pages 193–233, 1994.
- [11] M. Garland and P. Heckbert. Fast polygonal approximation of terrains and height fields. Technical Report CMU-CS-95-181, Carnegie Mellon University, 1995.
- [12] S. Geman and D. Geman. Stochastic relaxation, gibbs distributions, and the bayesian restoration of images. *IEEE Transactions on Pattern Analysis and Machine Intelligence*, 6(6):721–741, 1984.
- [13] N. Giordana and W. Pieczynski. Estimation of generalized multisensor hidden markov chains and unsupervised image segmentation. *IEEE Transaction on Pattern Analysis and Machine Intelligence*, 19(5):465–475, 1997.
- [14] L. Guillaume, D. Florent, and B. Atila. Curvature tensor based triangle mesh segmentation with boundary rectification. In *Computer Graphics International*. IEEE Computer Society, 16-19 Jun 2004.
- [15] S. Lakshmanan and H. Derin. Simultaneous parameter estimation and segmentation of gibbs random fields using simulated annealing. *IEEE Transactions on Pattern Analysis Machine Intelligence*, 11(8):799–813, 1989.
- [16] J. Marroquin, S. Mitter, and T. Poggio. Probabilistic solution of ill-posed problems in computacional vision. *The American Statistician*, 82:76–89, March 1987.
- [17] G. Miller, E. Steven, and N. Walkington. When and why Ruppert’s algorithm works. In *Proceedings of the 12th International Meshing Roundtable*, pages 91–102. Sandia National Laboratory, September 2003.
- [18] J. Rajapakse, J. Giedd, and J. Rapoport. Statistical approach to segmentation of single-channel cerebral mr images. *IEEE Transactions on Medical Imaging*, 16(2), April 1997.
- [19] A. Rosholm. *Statistical Methods for Segmentation and Classification of Images*. PhD thesis, Technical University of Denmark, 1997.
- [20] J. Ruppert. A delaunay refinement algorithm for quality 2-dimensional mesh generation. *J. Algorithms*, 18(3):548–585, 1995.
- [21] W. Schwartz and H. Pedrini. Segmentação de imagens de terrenos baseada na associação de características de texturas com dependência espacial modelada por campo aleatório de markov. Goiânia, 2005. XII Simpósio Brasileiro de Sensoriamento Remoto.
- [22] H. Sheshadri and A. Kandaswamy. Detection of breast cancer by mammogram image segmentation. *Journal of Cancer Research and Therapeutics*, 1(4):232–234, 2005.
- [23] C. Yonggfeng and S. Hong. An unsupervised segmentation method mased on mpm for sar images. *IEEE Geoscience and Remote Sensing Letters*, 2(1):55–60, 2005.
- [24] H. Zhang and R. Liu. Mesh segmentation via recursive and visually salient spectral cuts. In *Vision, Modeling, and Visualization*. Erlangen, 16-18 Nov 2005.
- [25] Y. Zhidong, S. Kumar, and C.-C. Kuo. Mesh segmentation schemes for error resilient coding of 3-d graphic models. *IEEE Trans. on Circuits and Systems for Video Technology*, 15(1):138–144, 2005.